Available online at www.sciencedirect.com

ScienceDirect

Procedia Engineering 160 (2016) 231 – 238

Procedia Engineering

www.elsevier.com/locate/procedia

XVIII International Colloquium on Mechanical Fatigue of Metals (ICMFM XVIII)

# Microscopic Damage Evolution during Very High Cycle Fatigue (VHCF) of Tempered Martensitic Steel

Ulrich Krupp[a]*, Alexander Giertler[a], Kevin Koschella[a]

[a]*Institute for Materials Design and Structural Integrity, University of Applied Sciences Osnabrück, 49009 Osnabrück, Germany*

**Abstract**

Dimensioning of high-strength steels relies on the knowledge of Wöhler-type S/N data and the assumption of a fatigue limit for applications where the number of load cycles exceeds $10^7$. Very high cycle fatigue (VHCF) experiments applied to a 0.5C-1.25Cr-Mo tempered steel (German designation: 50CrMo4) revealed surface crack initiation at prior austenite grain boundaries in medium strength condition (37HRC) and internal crack initiation at non-metallic inclusions at high strength condition (48HRC). Despite the formation of small cracks during cycling up to $10^9$ cycles, it seems that the medium strength condition exhibits a real fatigue limit. Application of automated electron back-scattered diffraction (EBSD) within the shallow-notched area of electro-polished fatigue specimens had shown that prior austenite grain boundaries act as effective obstacles to crack propagation. High resolution thermography during cycling of the specimens allowed the identification of local plasticity, which led to crack initiation at a later stage of the fatigue life. It was found that Cr segregation rows play a decisive role in the crack initiation process. By means of high-resolution electron microscopy in combination with focused ion beam milling (FIB), evolution of cyclic plasticity and crack initiation was correlated with the material's microstructure. The results are discussed in terms of the completely different crack initiation mechanisms of medium and high strength variants of the same steel. EBSD and crack propagation data are used to adapt numerical modeling tools to predict crack initiation and short crack propagation.


Peer-review under responsibility of the University of Oviedo

*Keywords:* VHCF; crack initiation, modeling, tempered steel

* Corresponding author. Tel.: +49 5412 9692188.
*E-mail address:* u.krupp@hs-osnabrueck.de


Peer-review under responsibility of the University of Oviedo
doi:10.1016/j.proeng.2016.08.885

## 1. Introduction

Tempered martensitic steels are standard materials for any application involving cyclic loading conditions at high stress levels and, at the same time, high numbers of cycles, e.g., components of the power train and the fuel injection system of cars or load transmission systems in power generation. Today, structural integrity concepts are generally based on the total-life Wöhler concept using S/N curves and the existence of a fatigue limit, respectively. However, very high cycle fatigue (VHCF) research revealed that high-strength steels tend to fail by fatigue fracture beyond $10^7$ cycles at stress values below the classical fatigue limit [1]. The micro mechanisms of fatigue in the VHCF regime are not fully understood yet. In the case of tempered martensitic steels, the mechanisms are closely related to variations in the hierarchical arrangement of microstructural features. During the first heat treatment step, martensitic steels are normalized in the fcc austenite regime. By quenching in water or oil, carbon diffusion is suppressed and instead of fcc austenite to bcc ferrite transition a diffusion-less martensitic transformation is promoted. This transformation initiates at the austenite grain boundaries as needle-shaped tetragonal (bct) martensite laths (cf. Fig. 3a), where the crystallographic relationship between the bct laths and the fcc parent austenite grains follows 24 possible variants, according to the Kurdjumov-Sachs relationship [2]. Tempering at temperatures between about 200°C and 600°C allows carbon to diffuse out of supersaturation in the martensite leading to the formation of Fe,Cr carbides. Therefore, the microstructure hierarchy is represented by (i) prior austenite grains, (ii) martensite packets, and (iii) martensite blocks containing the laths and the carbides [2]. Furthermore, tempered steels contain non-metallic inclusions (e.g., $Al_2O_3$, Ti(C,N)) , which act as internal crack nucleation sites during VHCF. According to Murakami [3], the fatigue limit $\sigma_{FL}$ of a steel with a Vickers hardness HV can be correlated to the inclusion size (area):

$$\sigma_{FL} = \frac{C(HV+120)}{\left(\sqrt{area}\right)^{1/6}}\left(\frac{1-R}{2}\right)^{\alpha} \tag{1}$$

where $R$ is the stress ratio, $C$ and $\alpha$ are constants representing the inclusion site and the material's hardness. A closer analysis of the internal crack initiation sites revealed the formation of a fine-granular area (FGA) around the inclusion. According to Grad et al. [4], the FGA is a result of cyclic micro plasticity in the vicinity of the inclusion leading to local recrystallization. Since the threshold stress intensity range for fatigue crack initiation decreases with decreasing grain size, the recrystallization zone is followed by local cracking forming the FGA. Once the FGA-induced stress intensity range exceeds the threshold value $\Delta K_{th}$ a technical fatigue crack is initiated. In contrast to that, martensitic steels tempered at higher temperatures and hence exhibiting a lower strength tend to VHCF crack initiation at the surface at locations fairly independent of the non-metallic inclusion sites. Obviously, wide-spread plastic slip at surface stress raisers, like prior austenite grain boundaries, cause the formation of protrusion bands parallel to the martensite laths.

**Nomenclature**

| | |
|---|---|
| a | crack length |
| $C$ | constant, defining inclusion sites at ($C$=1.43) or underneath ($C$=1.56) the surface, or within the bulk ($C$=1.41) |
| $N$ | number of cycles |
| $R_{p0.01}$ | (cyclic) 0.01% yield strength |
| $\alpha$ | exponent of the Murakami equation (1) |
| $\varepsilon$ | total strain |
| $\lambda$ | irreversible part of the crack tip shear displacement |
| $\sigma_{FL}$ | fatigue limit |
| $\sigma_a$ | stress amplitude |
| $\tau_c$ | critical shear stress |
| $\Delta$CTSD | range of the crack tip shear displacement |
| $\Delta K_{th}$ | threshold of the stress intensity range |

Such a behavior was reported and used for numerical modeling, e.g., by Brückner-Foit and Huang [5], Glodez et al. [6] and Mikkola et al. [7], where the prior austenite grain boundaries are considered as barriers to fatigue crack propagation. It is subject of the present work to understand the micro mechanisms of local cyclic plasticity and crack initiation, as well as the conditions for propagation or non-propagation of microstructurally short fatigue cracks in order to develop a mechanism-based model for VHCF life assessment based on the concept of microstructural barriers (cf. [8,9]).

## 2. Experimental

Subject of the present work is a 0.5C-1.25Cr-Mo tempered steel (German designation: 50CrMo4) with a chemical composition as given in Table 1. In the as-received condition the material was given a normalizing heat treatment at 850°C (0.5h) followed by quenching in oil and a tempering treatment at 550°C (1h) resulting in a hardness of 37HRC and a grain size of 12µm. In addition to that, some specimens were given a grain coarsening treatment prior to normalizing (for cyclic Hall-Petch analysis), and some specimens were tempered at lower temperatures to obtain a higher strength level of 48HRC (resulting in internal VHCF crack initiation, not reported in this study).

Table 1. Chemical composition of the tempered 50CrMo4 (in wt.%).

| Material | C | Cr | Mo | Mn | P | S | Fe |
|---|---|---|---|---|---|---|---|
| 50CrMo4 | 0.48 | 1.00 | 0.18 | 0.71 | 0.013 | 0.010 | bal. |

Fatigue specimens were machined according to Fig. 1b and Fig. 2b. The gage length was electropolished to allow fatigue damage monitoring by light and electron microscopy, as well as by high resolution thermography (ImageIR 8380 hp, 2µm pixel size, Fig. 1a). VHCF testing was carried out under stress control at fully-reversed cycling ($R$=-1) using both, a 20kHz ultrasonic testing system (type BOKU Vienna, Fig. 2a) and a 400Hz resonance testing machine (Rumul Testronic, Fig. 1a). Microstructural features of fatigue damage were identified by means of high-resolution scanning electron microscopy (SEM, ZEISS Auriga FEG) in combination with automated electron back scatter diffraction (EBSD, Oxford Aztec) and focused ion beam milling (FIB).

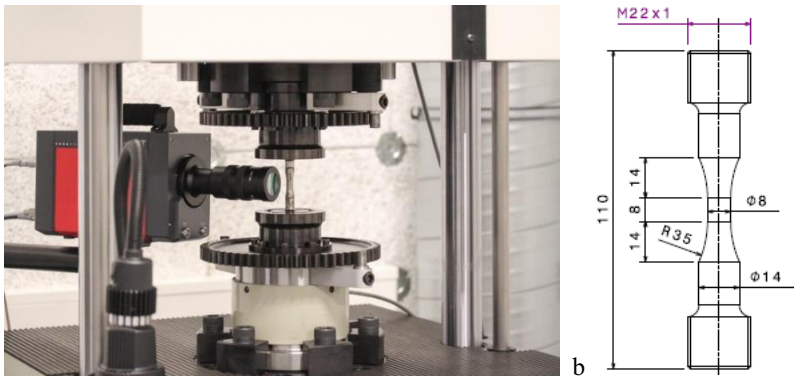


Fig. 1. VHCF testing: (a) resonance testing system RUMUL Testronic with high-resolution thermography camera, and (b) respective specimen geometry.

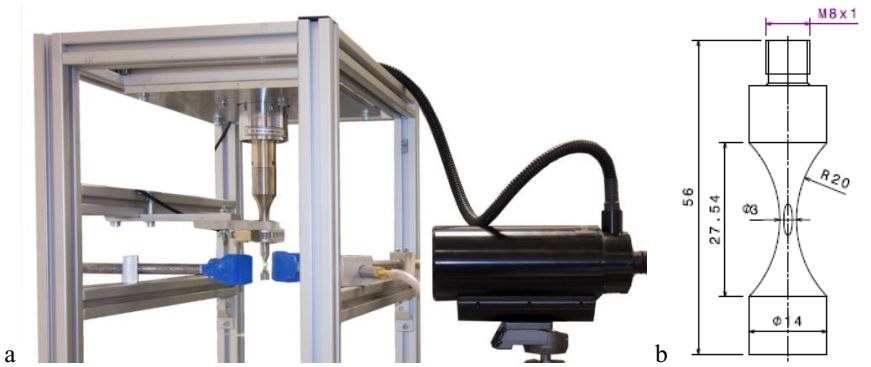


Fig. 2. VHCF testing: (a) ultrasonic fatigue testing system type BOKU Vienna, and (b) respective specimen geometry with shallow notch in the center of the specimen gage length for monitoring of fatigue damage.

## 3. Results

The microstructure of the tempered martensitic steel 50CrMo4 is represented as EBSD inverse pole figure map in Fig. 3a. The colors represent the crystallographic orientations of the various martensite variants. According to the KS relationship, these orientations can be used to reconstruct the prior austenite grains (Fig. 3b) by using the software package ARPGE [10]. Knowledge of the crystallographic orientations allows to account for the elastic anisotropy of the bcc martensite blocks within a FEM simulation of the microstructure given in the highlighted rectangle in Fig. 3a. The results shown Fig. 3c reveal a plastic strain concentration at the prior austenite grain boundaries.

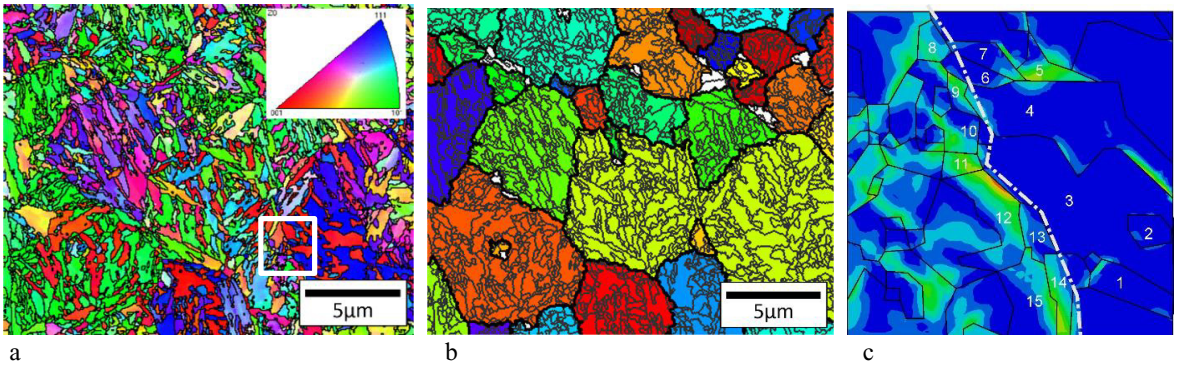


Figure 3. (a) Inverse pole figure mapping of the 50CrMo4 steel in transversal direction, (b) automated parent austenite grain reconstruction, (c) FE simulation of accumulated plastic strain $\gamma_{acc}$ at {110}<111> slip systems within the section highlighted in (a).

The fatigue life data are summarized in Fig. 4, representing a Wöhler-type S-N diagram of the tempered steel 50CrMo4. In the medium strength condition (37HRC), no fracture at numbers of cycles exceeding $10^7$ was observed, despite the fact that in any case cracks were identified (cf. Fig. 5). The data in Fig. 4 reveal a pronounced difference in fatigue strength between the tests carried out at 95Hz and the ultrasonic tests carried out at 20,000Hz. This frequency effect can be considered as a strain rate effect (cf. [11]): At 20,000Hz a strain rate in the order of approximately $d\varepsilon/dt=10^2 s^{-1}$ may shift the critical temperature, where thermal activation of the Peierls stress is a negligible contribution to the critical shear stress $\tau_c$. For high-strength steels this effect is not observed because of the overall higher level of $\tau_c$.

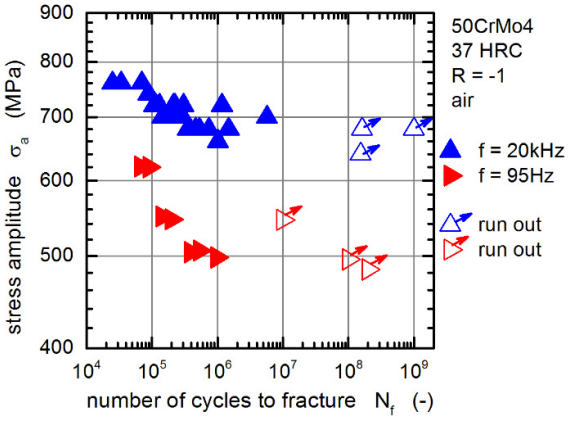


Figure 4. S-N diagram showing the different behaviour for 20kHz and 95Hz testing frequency.

Micro mechanisms of VHCF damage seem to be determined by cyclic irreversibility leading to protrusion bands of a similar appearance than persistent slip bands (PSB). The protrusion bands shown in Fig. 5 follow the orientation of the martensite laths. There is an obvious interaction between the protrusion bands and the prior austenite grain boundaries, as it can be seen in Fig. 5a. Here, the bands are piled up at the boundary causing intergranular crack formation. Protrusion bands formed within the prior austenite grains leads to the initiation of very shallow transgranular cracks, as it was revealed by FIB section across the protrusion band (Fig. 5b).

It is worth mentioning that in both cases the specimen did not fail up to $10^9$ cycles. Obviously, the existing cracks are permanently blocked by microstructural barriers, i.e., the material exhibits a fatigue limit.

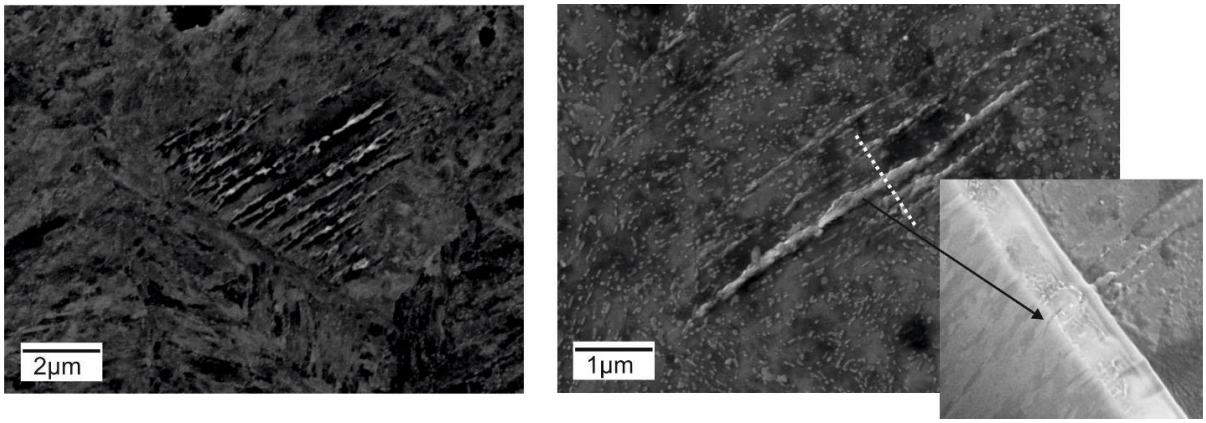


Figure 5. Surface micrographs of VHCF-loaded specimens of 50CrMo4 ($\sigma_a$=640MPa, $N$=1.5·10$^8$): (a) protrusion bands piling up at a prior austenite grain boundary, (b) protrusion bands within a prior austenite grain aligned between martensite blocks (containing the small Fe,Cr carbides), the FIB section reveals a shallow fatigue crack (arrow).

From various earlier studies (e.g. [12]) it is known that accumulated plastic strain gives rise to a temperature increase that can be measured by carefully attaching thermocouples within and without the gauge length of a fatigue specimen. By means of load increase tests, the onset of plastic deformation can be evaluated by monitoring the

temperature change and the fatigue limit can be estimated. The example in Fig. 6 shows the thermographically measured temperature across the specimen surface.

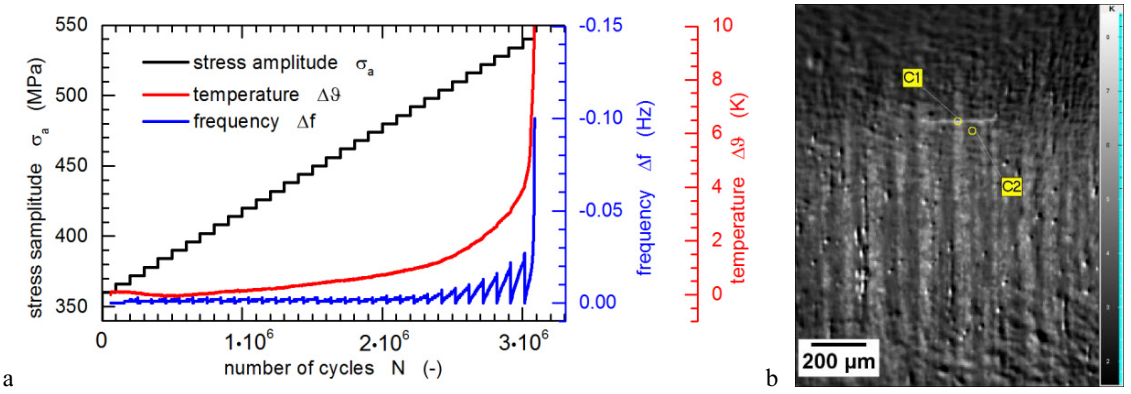


Figure 6. Thermographic analysis of fatigue damage: (a) stepwise load increase test and respective specimen response plotted as the change in temperature and resonance frequency, (b) thermogram of a fatigue specimen after $3 \cdot 10^6$ load cycles.

The detailed evaluation of thermographic data shows after a certain temperature decrease (due to the thermoelastic effect) a set-in of a continuous temperature increase starting at about 700,000 cycles – corresponding to a stress amplitude of about $\sigma_a$=396MPa. This value is well below the identified fatigue limit (approximately $\sigma_{FL}$=490MPa, see Fig. 4). At $N$=$2.4 \cdot 10^6$ cycles, the slope of the temperature vs number of cycles increases strongly due to fatigue crack initiation. The intersection of the secants of the two slopes yields an estimative value for the fatigue limit of $\sigma_{FL}$=483MPa, which is in good agreement with the 95kHz data in Fig. 4.

The data in Fig. 6a represent the temperature evolution at the crack initiation site, and were obtained from the recorded temperature distribution across the gage length vs. the time (a snap shot is shown in Fig. 6b). A ribbon-like structure was detected, where the light grey bands show a somewhat higher temperature increase than the darker bands. Correspondingly, a higher density of protrusion bands and the crack initiation site were found in the warmer areas (see "C1" in Fig. 6b). A more detailed analysis by energy dispersive X-ray spectroscopy (EDS) of the bands (cf. [13]) revealed small Cr segregations within the darker bands, a phenomenon that is known as microsegregation banding in hot rolled steels (cf. [14])..

## 4. Discussion and Modeling Approach

The VHCF damage behavior of tempered martensitic steels depends on the strength and the microstructure heterogeneity of the material. While high-strength steels tend to internal crack initiation at non-metallic inclusion, cyclic plasticity in medium-strength steels manifests itself in the formation of protrusion bands at sites with (i) stress concentration due to elastic anisotropy of neighboring grains, and (ii) low strength due to a lower Cr level and/or lower density of Fe,Cr carbides. The protrusion bands follow the orientation of the martensite laths/blocks and are blocked by the adjacent prior austenite grain boundaries, as it is schematically shown in Fig. 7a. According to earlier work (cf. [8,9]), the shear displacement field along the protrusion bands is calculated numerically by the boundary element approach. The irreversible part ($\lambda$) of the cyclic crack tip shear displacement range ΔCTSD is considered as crack driving force, while the shear displacement field (yield strip) is blocked by the prior austenite grain boundaries.

$$\frac{da}{dN} = \lambda \cdot \Delta CTSD \tag{2}$$

The barrier efficiency of these boundaries have been determined by evaluating the cyclic 0.01 yield strength ($R_{p0.01}$ cyclic) as a function of the prior austenite grain size. $R_{p0.01}$ cyclic has been determined from cyclic stress strain curves (CSSC, Fig. 7b) obtained from incremental step tests (IST).

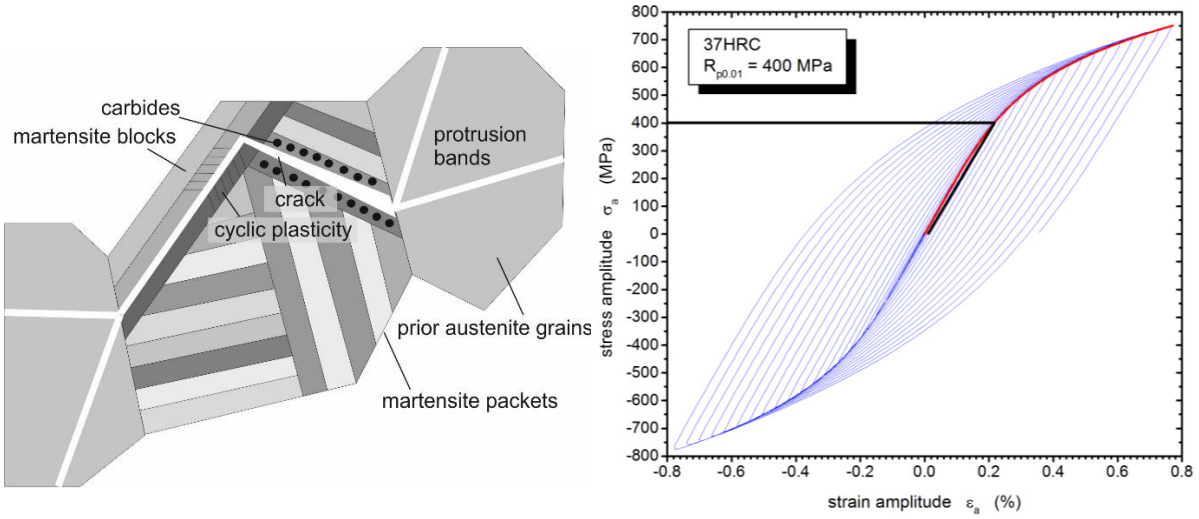


a b

Figure 7. Modelling microcrack propagation in tempered steel: (a) schematic representation of the modelling concept and (b) cyclic stress strain curve (CSSC) of the tempered steel 50CrMo4 in the as-received condition (37HRC).

Preliminary results yield a cyclic friction strength of $\tau_{cfr}$=304MPa, and a barrier strength (cyclic Hall-Petch constant) of $k_c$=9.1MPam$^{-1/2}$. The 0.01 cyclic yield strength of the as received materials $R_{p0.01}$ cyclic=400MPa corresponds with the value found for the onset of temperature increase $\sigma_a$=396MPa as an indication of first plasticity in Fig. 6a.

It is the subject of ongoing work to evaluate the mode of cyclic plasticity and characteristic dislocation arrangements in the martensite blocks that contribute to the shear deformation within the identified protrusion bands and to implement this in the modeling concept.

## 5. Conclusions

The very high cycle fatigue (VHCF) behavior of tempered steel has been studied by ultrasonic and resonance testing at frequencies of 95Hz and 20,000Hz, respectively. At medium hardness level (37HRC), the fatigue strength of the steel depends on the strain-rate and is substantially higher at 20,000Hz. On a microstructural length scale, VHCF damage manifests itself in the formation of protrusion bands that increase in density and cause the formation of shallow fatigue cracks. Alternatively, the protrusion bands can be piled up at the prior austenite grain boundaries, leading to intergranular separation. Damage in form of protrusion bands is promoted by Cr depleted segregation bands that show a slightly larger activity in cyclic plasticity as it was shown by high-resolution thermography.

However, up to $10^9$ cycles, these cracks did not overcome microstructural barriers and the materials seems to exhibit a fatigue limit. The barrier strength of the prior austenite grain boundaries has been estimated experimentally by incrementals step tests (IST) carried out on specimens of various prior austenite grain sizes. The respective strength data are used for numerical simulation of propagating and non-propagating VHCF cracks.

## Acknowledgements

The financial support of the project MICROLIFE by the German Ministry of Education and Research (BMBF) and the supply of test materials by Robert Bosch GmbH are gratefully acknowledged. Furthermore, the authors acknowledge the support by P. Hilgendorf in performing FEM simulations.

## References

[1] C. Bathias, P.C. Paris, Gigacycle Fatigue in Mechanical Practice CRC Press, New York, 2004.
[2] H. Kitahara, R. Ueji, N. Tsuji, Y. Minamino, Acta Mater. 54 (2006) 1279.
[3] Y. Murakami, M. Endo, Intl. J. Fatigue 16 (1994) 163.
[4] P. Grad, B. Reuscher, A. Brodyanski, M. Kopnarski, E. Kerscher, Scripta Mater. 67 (2012) 838.
[5] A. Brückner-Foit, X. Huang, Intl. J. Fatigue 28 (2006) 963.
[6] S. Glodez, N. Jezerni, J. Kramberger, T. Lassen, Adv. Engng Software 41 (2010) 823.
[7] E. Mikkola, G. Marquis, J. Solin, Intl. J. Fatigue 41 (2012) 64.
[8] U. Krupp, Fatigue Crack Propagation in Metals and Alloys, Wiley VCH, Weinheim, 2007.
[9] B. Künkler, O. Düber, P. Köster, U. Krupp, C.-P. Fritzen, H.-J. Christ, Engng Fract. Mech. 75 (2008) 715.
[10] C. Cayron, J. Appl. Cryst. 40 (2007) 1183.
[11] J. Bach, J.J. Möller, M. Göken, E. Bitzek, H.W. Höppe, Intl. J. Fatigue (2016) in press.
[12] B. Yang, G. Wang, W.H. Peter, P.K. Liaw, R.A. Buchanan, D.E. Fielden, Y. Yokoyama, J.Y. Huang, R.C. Kuo, J.G. Huang, D.L. Klarstrom, Met. Mater. Trans. A 35 (2004) 15.
[13] A. Giertler, U. Krupp, Scripta Mater, submitted.
[14] S.E. Offermann, N.H. van Dijk, T. Rekveldt, J. Sietsma, S. van der Zwaag, Mater. Sci. Techn. 18 (2002) 297.